Research Article Vol. 34, No. 7 / 6 Apr 2026 / Optics Express 12479
Optics EXPRESS

Temperature control and sample damage mitigation in static and transient soft X-ray experiments using flexible sample cells

Richard Gnewkow,[1,3,†,*] Daniel Grötzsch,[1,†] Jonas Kaiser,[1,2] Nele Bukowski,[1,3] Mattis Fondell,[4] Sebastian Eckert,[4] Holger Stiel,[1,5] Thomas Charles Rossi,[6] Birgit Kanngießer,[1,3] and Ioanna Mantouvalou[1,3]

[1]*Institute for Physics and Astronomy, Technische Universität Berlin, Berlin, Germany*
[2]*Current affiliation: Potsdam Institute for Climate Impact Research (PIK) e. V., Germany*
[3]*Combined X-ray Methods at BLiX and BESSY II - SyncLab, Helmholtz-Zentrum Berlin für Materialien und Energie GmbH, Berlin, Germany*
[4]*Helmholtz-Zentrum Berlin für Materialien und Energie GmbH, Institute for Methods and Instrumentation for Synchrotron Radiation Research, Berlin, Germany*
[5]*Max-Born-Institut für Nichtlineare Optik und Kurzzeitspektroskopie, 12489 Berlin, Germany*
[6]*Department of Atomic-Scale Dynamics in Light-Energy Conversion (PS-ADLU), Helmholtz-Zentrum Berlin für Materialien und Energie GmbH, Berlin, Germany*
[†]These authors contributed equally.
[*]*richard.gnewkow@tu-berlin.de*

Abstract: Pump-probe X-ray spectroscopy is a powerful technique for probing how light excitation affects the electronic and lattice structure of molecules and materials. In solid samples, laser excitation inherently leads to lattice heating, which can damage samples and distort transient spectra, especially at the high repetition rates typical of large-scale facilities. To address these challenges, we present two in-vacuum sample cells to mitigate sample damage and to assess the contribution of lattice heating to transient X-ray signals. The first cell enables controlled sample heating for static temperature-dependent X-ray experiments. The second cell uses gas flow to enhance heat dissipation, resulting in a significant reduction of heat accumulation and laser- and X-ray-induced sample damage. We introduce a methodology to estimate sample heating across a wide range of laser parameters, intended as a practical tool to optimize XTA experiments.

1. Introduction to soft X-ray absorption spectroscopy and X-ray transient absorption spectroscopy

X-ray absorption spectroscopy (XAS) is a widely used element- and site-specific technique to investigate the electronic and geometric structure of matter. In the soft X-ray range the K-edges of light elements such as carbon, nitrogen and oxygen and the L-edges of 3d transition metals are accessible between ~280 and ~1100 eV. This energy range enables the investigation of the primary building blocks of organic complexes or active sites in catalysts and metalloproteins. For photoactive materials, the structure-function relationship can be further investigated by studying the dynamic changes after photoexcitation using X-ray transient absorption (XTA) spectroscopy. Understanding the excitation and relaxation pathways is important for systems in catalysis [1], surface science [2] or organic photovoltaics [3].

1.1. Sample heating in XTA measurements: mitigation and quantification

Most XTA experiments are conducted in the pump-probe (stroboscopic) scheme in which a laser pulse excites a sample and an X-ray pulse probes its transient state at different time delays. The

#584000 https://doi.org/10.1364/OE.584000
Journal © 2026 Received 20 Nov 2025; revised 26 Jan 2026; accepted 30 Jan 2026; published 27 Mar 2026

Optics EXPRESS

laser-induced absorption change (A_{pumped}) is compared to the unexcited ground state absorption ($A_{unpumped}$) in the form of the absorption difference $\Delta A = A_{pumped} - A_{unpumped}$. In typical thin-film XTA experiments, an absorbed fluence of approximately 1 mJ/cm^2 [4] is necessary to achieve a sufficient excitation density. Since most of the absorbed laser energy is ultimately converted into heat, each laser pulse increases the sample temperature. These elevated sample temperatures in the pumped measurement can either cause irreversible sample degradation or reversible thermal effects, manifesting as peak shifts, broadening or intensity changes [5] that overlap with signals arising from non-thermal perturbations of the electronic and lattice structure of materials. When the hotter, pumped measurements are compared with the cooler unpumped measurements, the temperature difference can distort the non-thermal XTA signal and lead to wrong conclusions if thermal effects or sample degradation are ignored. Sample heating is especially critical in soft X-ray transmission experiments, where a vacuum environment and thin samples and substrates, typically below a micrometer, are required, limiting heat dissipation.

In pump-probe experiments, two laser heating regimes can be distinguished: *dynamic* and *static* heating. In the *dynamic* regime, each laser pulse transiently increases the sample temperature, but the time between consecutive pulses is long enough for the sample to cool back to ambient temperature (orange curve, Fig. 1(a)). This situation occurs in low-repetition-rate experiments or for high sample heat dissipation. In ultrafast experiments with sufficient time resolution, the temperature increase after laser excitation cannot be assumed to be a simple step function. Instead, the electron and phonon temperatures are out of equilibrium for several picoseconds to tens of picoseconds [6]. Independent of the time resolution of the experiment, the rapid temperature increase caused by each laser pulse is, in first approximation, independent of the sample substrate and thus unavoidable.

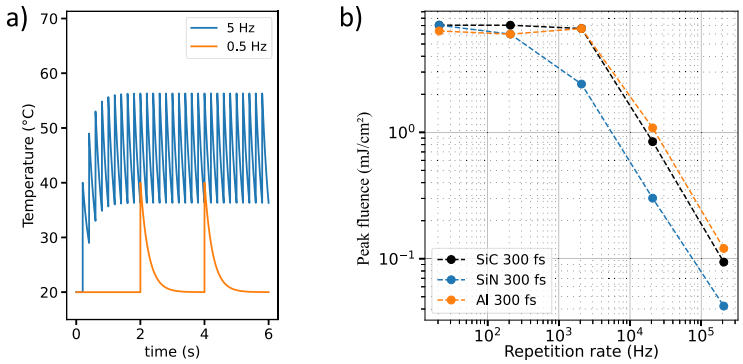

Fig. 1. a) Simulated heat build-up after laser excitation in a purely dynamic regime (orange curve) and in a static regime (blue curve). b) Maximum fluence without transmission change in mJ/cm^2 as a function of repetition rate for 140 nm TAP on SiN_x/Al/SiC substrates, 300 fs, 515 nm, 200 µm^2 FWHM beam diameter.

For higher repetition rates or under poor heat dissipation conditions, the sample does not cool back to ambient temperature between consecutive laser pulses, leading to cumulative heat build-up referred to as *static* heating (blue curve, Fig. 1(a)). In this regime, the samples reach a quasi-equilibrium hot state, which undermines measurements intended to probe materials under ambient conditions and can even cause sample damage. Together, these challenges call for (1) controlled-temperature XAS measurements to enable accurate interpretation of time-resolved spectra and (2) experimental strategies to mitigate heat accumulation in XTA measurements of thin samples.

Elevated sample temperatures caused by static heating can be minimized, but dynamic heating cannot be prevented. As a result, thermal signals are inherently present in XTA experiments and

Optics EXPRESS

must be considered during data interpretation. Several strategies have been proposed to account for sample heating. A common approach is to estimate and subtract thermal contributions from the XTA spectrum, either by measuring XAS spectra of statically heated samples [3] or by using data collected at negative delays [3,7] (i.e., shortly before laser excitation). However, the applicability of these methods is limited and static heating can lead to very high temperatures that may irreversibly damage the sample through oxidation [8] or interaction with the substrate [9]. To maintain high laser repetition rates while minimizing heating, efficient methods to reduce static heating are required. One strategy is to modify the measurement scheme, such as rapid sample movement [10] or reducing the time difference between pumped and unpumped measurements [11]. Alternatively, heat dissipation can be improved by using substrates with high thermal conductivity, though this approach often constrains the achievable crystallinity of the thin films and the effectiveness is sample-dependent [12]. A smaller laser focus size can also improve heat dissipation [13], but this requires a correspondingly smaller X-ray spot size, which increases the X-ray dose and therefore X-ray sample damage. Additionally, the spatial overlap between laser and X-rays becomes more sensitive to small drifts.

Another approach to mitigate static heating in high-repetition rate XTA experiments is to utilize continuous gas flow to cool the sample. Several gas cooling strategies have been explored for XTA experiments. One approach uses a small gas-filled sample chamber at ambient pressure, separated from the vacuum chamber by two silicon nitride windows [14]. While this allows for easy sample exchange, the long beam path through gas at ambient pressure causes significant absorption and the large pressure difference requires thick windows, further increasing attenuation. An alternative method is to continuously blow gas into the vacuum chamber and onto the sample [15], thereby increasing the chamber pressure. This approach is straightforward to implement and does not require additional X-ray windows, but may be incompatible with some experimental setups.

In this work, we develop a third approach in which the sample is enclosed inside a compact gas-filled cell [16]. This configuration provides efficient cooling without excessive X-ray absorption by the cell windows and the gas. The low setup constraints make it suitable for high-repetition-rate XTA measurements.

We first present the effects of different sample substrates on the laser damage threshold of an organic thin film (2,7,12,17-Tetra-tert-butyl-5,10,15,20-tetraaza-21H,23H-porphin, $C_{32}H_{42}N_8$, abbreviated as TAP). We follow this with a discussion of the design principles of two sample cells that together form a versatile toolkit for performing and interpreting XTA measurements. The first cell uses radiative heating to homogeneously raise the sample temperature, enabling temperature-dependent XAS measurements to isolate thermal effects in XTA signals. The second cell uses a continuous gas flow to allow for convective heat transfer and improve heat dissipation. Compared to earlier publications, the gas volume in this cell is fully separated from the surrounding vacuum, ensuring compatibility with high-vacuum beamline environments. Their suitability for different X-ray experiments is discussed based on results obtained for TAP and zinc oxide (ZnO) thin films.

2. Preliminary laser heating investigation

To demonstrate how the substrate properties affect sample heating in XTA experiments, we determine the damage threshold associated with laser-induced sample heating and subsequent sample evaporation. Three types of free-standing membranes are used: (i) 150 nm non-stoichiometric amorphous silicon nitride (SiN_x, from Norcada Inc.), (ii) 300 nm polycrystalline silicon carbide (SiC, from NTT-AT) and (iii) 150 nm aluminum. Reported thermal conductivities for thin films lie between 2-10 $Wm^{-1}K^{-1}$ for amorphous SiN_x [17–19] and 70 - 100 $Wm^{-1}K^{-1}$ for Al [18,20]. Values for SiC thin films scatter significantly due to strong dependence on the preparation process. Amorphous SiC exhibits conductivities as low as 1-1.5 $Wm^{-1}K^{-1}$ [21,22],

Optics EXPRESS

whereas crystalline films have values as high as 200 $Wm^{-1}K^{-1}$ for a thickness of 930 nm [23]. The thermal conductivity of the 300 nm polycrystalline SiC film used here is expected to lie between these two values.

A 140 nm thin film of TAP is used as a reference in our experiments, as previous work [24] has shown that laser excitation leads only to sample evaporation without causing sample degradation. For the in-vacuum experiment, the second harmonic (515 nm) of a laser system with 1030 nm wavelength, 300 fs pulse duration and variable repetition rate of up to 208 kHz (Pharos series from Light Conversion) is used for optical excitation. In the experiment, the sample transmission is measured and the maximum fluence without transmission change is determined as a function of laser repetition rate. Experimental details are provided in the SI.

At low repetition rates, no effect of substrate type or repetition rate is observed (Fig. 1(b)), indicating that dynamic heating from a single laser pulse determines the maximum fluence. For SiN_x membranes, the maximum fluence decreases above 700 Hz repetition rate, corresponding to the transition where static heating and the associated power density determine the sample temperature. For both higher conducting substrates, this transition occurs at approximately 2000Hz, an improvement by a factor of 3. This improvement remains nearly constant up to the maximum repetition rate of 208 kHz.

For a fluence of 1 mJ/cm^2 a maximum laser repetition rate of 10 kHz can be identified, even for the higher conducting substrates. This repetition rate is one to two orders of magnitude lower than the values of advanced HHG sources [25] and those of large-scale facilities [26]. Additionally, although the TAP sample is not destroyed at 10 kHz, it is heated almost to its evaporation temperature. It would therefore suffer from extreme static heating effects, leading to XTA measurements of hot samples that differ significantly from those at ambient temperature. Thus, a further reduction of the laser repetition rate is mandatory to remain in the dynamic heating regime, which severely reduces the achievable signal-to-noise ratio (SNR) in thin-film experiments.

3. Cell concepts and characterization

The two cells presented here are a development based on previous work. For the soft X-ray range, we have already developed cells for photon-in/photon-out experiments of solutions [27] and adsorbed molecules on substrates in a gaseous environment [28]. Most recently, a cell for temperature control of samples in the hard X-ray range was presented [29]. All these cells are designed to be interchangeable and flexibly used in both laboratory and large-scale facility setups.

The first cell (heating cell) is specifically designed to facilitate temperature-dependent XAS measurements and aid the interpretation of thermal signals in XTA measurements. Temperature control is achieved by surrounding the thin film inside a heated volume, where radiative heat exchange governs the thermal equilibration. The cell opening for the X-ray beam path is small relative to the heated cell surface to optimize radiative heat exchange. The second cell (gas cell) enables a continuous gas flow around a thin-film sample and is primarily designed to mitigate static heating in XTA experiments. We further show that the gas flow also reduces laser and X-ray-induced sample damage. Both cells have the same dimensions perpendicular to the X-ray beam, the same beam path and identical connection positions, allowing both cells to be easily exchanged.

3.1. Heating cell

The aluminum heating cell body (Fig. 2) measures $(30 \times 30 \times 90)$ mm and a 3.5 mm diameter hole provides a path for the X-ray beam. The cell length of 90 mm is a compromise between optimized radiative heat exchange and cell handling. A simple estimation yields a maximum deviation of 1 K between the enclosed sample membrane and a 200 °C cell body for 20 °C ambient temperature. More details about the cell are provided in the SI.

Optics EXPRESS

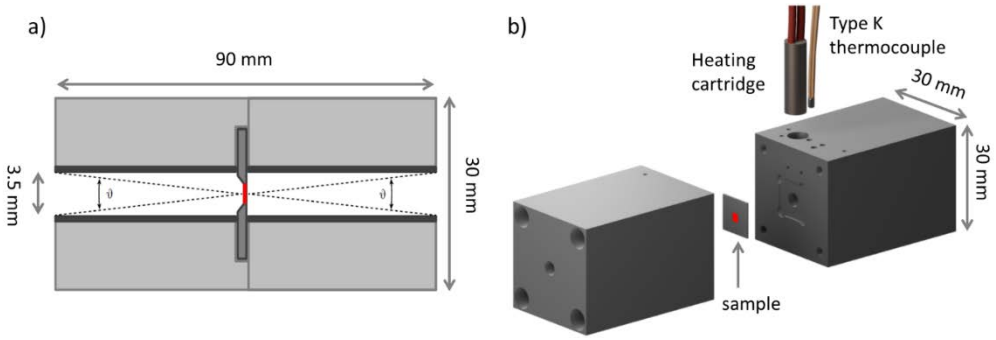

Fig. 2. a) Cross-section of a TAP sample (red) and its support frame (dark grey) centered in the heating cell (light grey) with opening angle $\vartheta \approx 4.5°$. The interior walls are coated with colloidal graphite (black). b) Exploded CAD drawing with heater and temperature probe.

The cell has a heating rate of around 6 °C/min and full thermalization with minimal overshoot (<1.5°C) is reached within 14 minutes after reaching the target temperature, being slightly faster at higher temperatures. Because the cell lacks active cooling and is thermally isolated from the sample holder, the natural cooling rate is slow, reaching about 0.2°C / min at 90°C. Once stabilized, a stable temperature is maintained for hours, with a standard deviation of the measured temperature of 0.02 °C and maximum deviations below 0.1 °C. With the aluminum body, the current temperature limit is 500 °C [29].

3.2. Characterization of the heating cell

To characterize the heating cell, a XAS setup [30,31] using a laser-produced plasma source was utilized. Briefly, the setup uses soft X-rays emitted from a plasma formed by the interaction of a high-intensity laser pulse with a solid target material (typically Cu or W). The emitted X-rays are transmitted through a sample and then dispersed by a reflection zone plate (RZP) onto a CCD detector. Here, we use RZPs on a curved substrate. These facilitate direct two-dimensional imaging of the sample's transmission in the 0th diffraction order shown in Fig. 3(a). In the first diffraction order, XAS spectra are obtained with an energy-resolving power of about 1000 [31].

To assess whether the heating of the film inside the cell is homogeneous, a 150 nm TAP film on 150 nm Al membrane is used. In the X-ray transmission experiment, the increase in transmission due to sample heating and subsequent evaporation is monitored. Figure 3(b) shows the heating protocol in black as well as the average transmission in the 0th order for the region indicated by the red box in (a). Figure 3(c) shows N K-edge XAS measurements in transmission (average of 100 single-shot images, 14 ms integration time each) in first order, conducted at time intervals marked with stars in (b). At 120°C, the TAP film is completely evaporated. During sample evaporation, a small transmission gradient is observed in the 0th order along the vertical and horizontal directions. The gradient can be described by a second-order polynomial centered on the $2 \times 2\,\mathrm{mm}^2$ membrane with a relative transmission difference between the center and the edges of the red box of up to 3%, indicating almost homogeneous sample heating. More information can be found in the SI.

3.3. Gas cell

The concept of gas cells is to surround the sample membrane with gas to allow for convection as an additional mechanism of heat exchange. Depending on the gas temperature, this can be used either to heat the sample or for sample cooling by flowing (below) ambient temperature gas over the sample membrane.

Optics EXPRESS

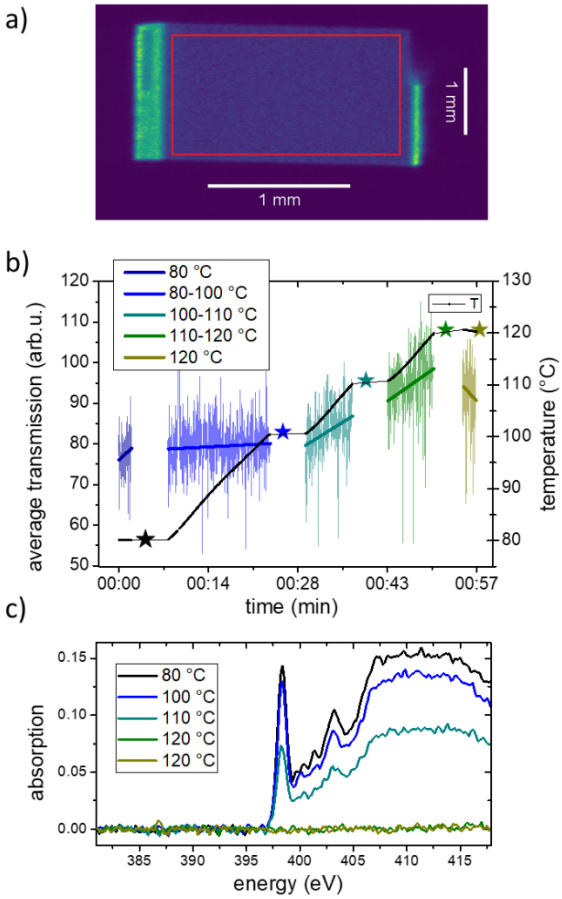

Fig. 3. a) Initial transmission through the $2 \times 2\,\mathrm{mm}^2$ TAP film measured in 0th diffraction order. The bright sections on the left and right sides are caused by total reflection at the RZP substrate. Only data from the RZP structure (red square) is used in the evaluation. b) Transmission in 0th order of the TAP film with an initial thickness of 150 nm as a function of time and temperature, c) Reduced absorption at the N K-edge due to sample evaporation for points in time indicated by the colored stars in b. At 120 °C, the complete TAP film is evaporated.

The gas cell body shown in Fig. 4 is made of aluminum and measures $(30 \times 30 \times 20)\ \mathrm{mm}^3$, with a 3.5 mm diameter hole for the X-ray beam path. The cell's upper temperature limit is 200 °C due to the fluoroelastomer (FKM) sealings and the pressure sensor.

In Fig. 4, two options for containing and guiding gas in the cell are illustrated. To separate the gas cell from the outer vacuum environment, commercially available SiN_x membranes are the most suitable due to their high mechanical strength and high transmission in the visible and UV regions, down to 275 nm. Figure 4(a) and 4(b) show the case, where the sample is deposited on one membrane (marked in red) and placed facing the inside of the cell and a second window encloses the small gas volume. Due to the pressure difference, the membranes bulge outward during the experiment with displacements of up to 70 µm [32] in the middle of the windows when large area membranes ($\sim\mathrm{mm}^2$) are used. For experiments where the sample must be flat, three membranes are used (Fig. 4(c) and (d)). Two outer windows separate the gas volume from the vacuum, and one serves as a substrate for the thin film inside the gas cell. The distance between

Optics EXPRESS

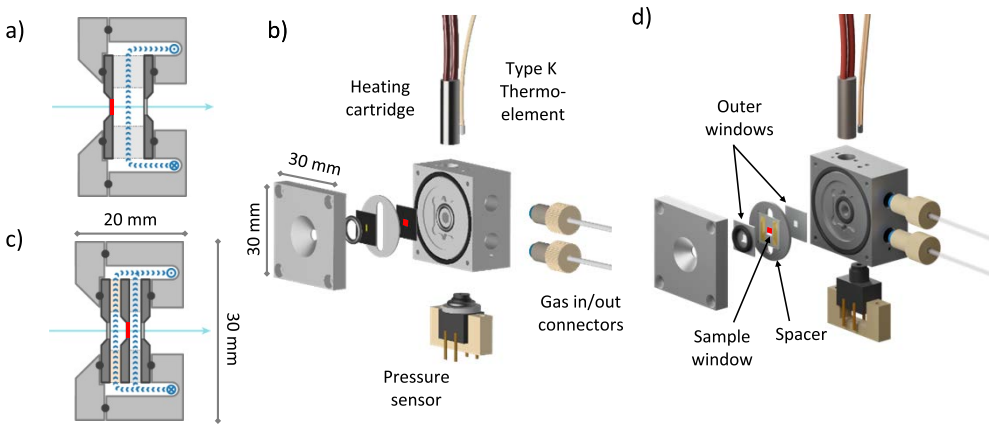

Fig. 4. a,c) Cross section of the X-ray path (cyan) through the cell and the gas flow (blue) in the cell (not to scale). The gas is contained by the cell body (grey) and the SiN_x frame(s) (dark grey), sealed by O-rings (black). The sample membrane is depicted in red. b,d) CAD drawing of the gas cell. The distance between the outer SiN_x frames is maintained by a metal spacer and, on one side, by Kapton tape (orange shaded areas) in the case of three frames.

the Si frames can be adjusted with a metal spacer and Kapton tape. To reduce the absorption by the gas, the X-ray path through the gas cell is minimized to about 1 mm. More information is supplied in the SI.

To facilitate efficient heat transport away from the sample membrane, a continuous and preferably turbulent flow of gas is desirable to break the boundary layer. The inner geometry of the cell body is therefore purposefully designed with right-angled turns to enhance turbulence in the gas flow. Typically, helium is used due to its low absorption in the soft X-ray and optical ranges, its high specific heat capacity and its low chemical reactivity.

3.4. Static heating and sample damage measurements

To test the performance of the gas cell, in-vacuum transmission measurements of a ZnO thin-film are performed at the UE52_SGM beamline [33] in the AXSYS-nmTransmission NEXAFS chamber of the synchrotron radiation source BESSY II operated by the Helmholtz-Zentrum Berlin. The measurement scheme is illustrated in Fig. 5(a). The total X-ray flux of the experiment is 2.4×10^{10} ph/s in 0.1% bandwidth [34] with an X-ray energy resolving power of 12000 and a focus size at the sample position of $50 \times 20\,\mu m^2$ $1/e^2$ [35], resulting in a peak X-ray power density of around $0.5\,W/cm^2$. The X-ray detector is a Si photodiode (Opto Diode, AXUV100AL) coated with 150 nm Al to block ambient and laser light, which records X-rays from the full filling pattern of the storage ring with an integration time of 0.2 seconds. This measurement scheme, using an ungated detector, records the effect of induced static heating in the sample. All measurements were performed at 537.4 eV, corresponding to the absorption maximum at the O K-edge of ZnO (Fig. 5(b)) and also the position that shows the highest static heating effect in the form of reduced absorption.

The 290 nm ZnO thin film sample is deposited by radio-frequency sputtering onto 200 nm and 50 nm SiN_x membranes. Two 150 nm SiN_x membranes are used as outer windows to seal the gas cell.

To induce static heating in the sample, the third harmonic (343 nm) of the same Pharos laser system described above was used with a reduced repetition rate of 10.4 or 52 kHz, a laser spot size on the sample of $81\,\mu m^2$ FWHM and four peak fluences of 0.02, 0.2, 1.3 and 4.1 mJ/cm^2. As the laser penetration depth of ZnO is 71 nm at 343 nm [35], the incident laser power is almost fully

Optics EXPRESS

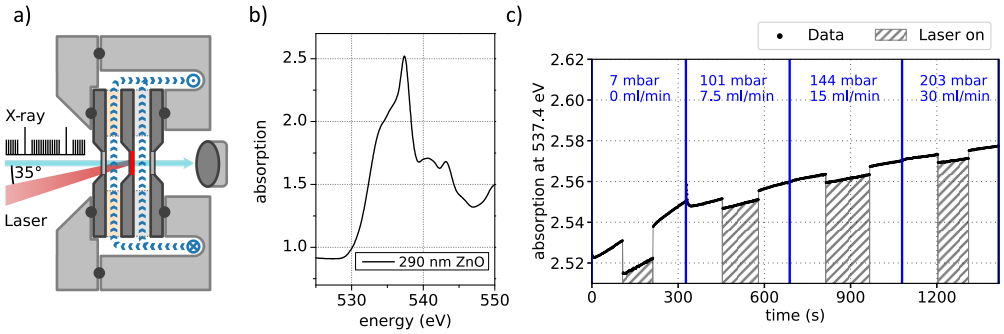

Fig. 5. a) Sketch of the measurement scheme, b) Static O K-edge XAS spectrum of a 290 nm ZnO thin-film sample on SiN_x membrane, c) ZnO absorption as a function of helium gas flow and pressure with laser on (dashed area) and laser off (solid area) for 10.4 kHz repetition rate and a peak fluence of 4.1 mJ/cm^2. During laser irradiation, the sample temperature increases rapidly, which leads to the observed decrease in absorption. The absorption recovers after the laser is switched off and the sample cools down to ambient temperature.

absorbed by the ZnO thin film, leading to a mean temperature increase of 8.9 K per 1 mJ/cm^2 peak fluence (see SI). Laser and soft X-ray beams have a 35° relative angle to each other.

In the experiment, helium was used with flow rates of 0, 7.5, 15, and 30 ml/min under normal reference conditions (DIN 1343), with a corresponding cell pressure of 7, 101, 144, and 203 mbar for a fully opened outlet valve. This is due to the small 1/16-inch gas tubing in the exhaust gas line, which prevents further reduction of the cell pressure. In future experiments, the diameter will be increased to 1/8-inch. Since the helium flow rate and cell pressure cannot be varied independently, all results are for the combined effect. The estimated helium flow speeds over the membranes are 0.0, 0.7, 0.9, and 1.3 m/s.

The aim of the experiment is to measure the isolated thermal signals induced by the pump laser and to characterize the effectiveness of the gas cell in suppressing them. Therefore, our measurements are static measurements in which the integrated temperature signal is compared to that of an unpumped sample. Measuring the thermal signal in this way has the benefit that the full ring current is utilized, which increases the flux by a factor of 75. Compared to the TAP sample, the thermal signal of the ZnO sample is not caused by evaporation, but rather the electronic structure, and therefore the XAS spectrum of ZnO is temperature-dependent. This effect is thus reversible and the sample signal recovers when the ZnO thin-film reaches ambient temperature.

Figure 5(c) exemplifies the integrated heating measurement of ZnO for the different gas cell parameters at a 10.4 kHz repetition rate and a peak fluence of 4.1 mJ/cm^2, corresponding to a peak power density of 42.6 W/cm^2. In the first section, from 0 to 328 s, the cell pressure is 7 mbar with no He flow and no UV excitation. At 107 s, the laser is switched on (dashed area) and the average absorption is abruptly reduced due to sample heating. At 202 s, the laser is switched off, the sample temperature equalizes rapidly to the ambient temperature and the absorption recovers. The procedure is repeated for different He flow rates, showing a continuous decrease of the thermal signal with increasing He flow rates. Because a higher flow rate results in a higher cell pressure, a small absorption jump is observed when the flow rate is increased. The absorption change can be reproduced assuming a 1.4 mm He path length, consistent with the cell's expected path length.

Besides the sudden absorption change caused by the laser, the measurement also shows a linear increase in absorption, as shown in Fig. 5(c). This is identified as permanent X-ray induced sample damage, as it does not recover even hours after the X-ray exposure. When the laser is incident on the sample, this continuous increase in absorption caused by X-ray damage is reduced,

Optics EXPRESS

indicating also laser-induced sample damage in the form of reduced absorption. Both X-ray and laser-induced sample damage are reduced at higher He flow rates. To avoid artifacts caused by X-ray and laser-induced sample damage, each measurement was performed on a fresh sample spot.

The results for X-ray and laser sample damage, as well as temperature-induced absorption changes for different flow cell and laser parameters, are shown in Fig. 6. X-ray sample damage, Fig. 6(a), is reproducible at different sample spots and has a value of 8×10^{-5} ΔA/s without helium flow and 7 mbar cell pressure, which is reduced by a factor of 4 for a flow rate of 30 ml/min. The decrease follows a single exponential decay with only small additional benefits for flow rates above 30 ml/min. We observed linear scaling of X-ray and laser damage with time, but for longer exposure times at the same sample position, a saturation is expected.

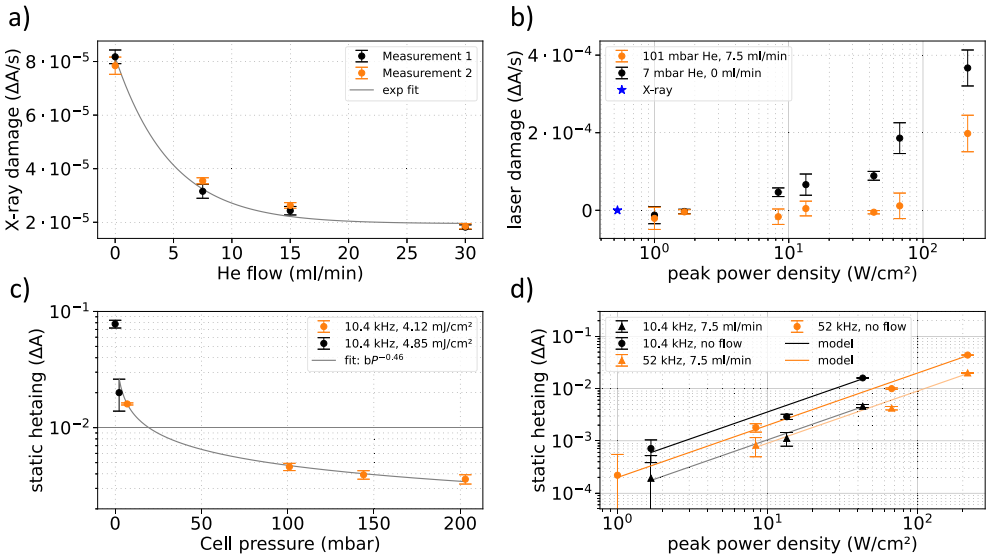

Fig. 6. a) X-ray damage as a function of He flow in the gas cell without laser. b) Laser damage as a function of peak power density with helium flow (orange) and without helium flow (black). c) Static heating as a function of cell pressure for the earlier experiment (black) and the current experiment (orange). d) Static heating as a function of the peak power density for 10.4 kHz (black) and 52 kHz (orange).

Laser damage, Fig. 6(b), is not detected for low peak power densities. With no helium flow, laser damage becomes significant at approximately 10 W/cm^2 and at approximately 200 W/cm^2 with a flow of 7.5 ml/min. As with the TAP sample, the laser damage is likely caused by elevated sample temperatures, which become significant only above a threshold power density. Since a single laser pulse leads to insufficient heating, only heat accumulation due to static heating causes laser damage. This explains the plateau at low peak power densities and the reduced laser damage for He flow due to better sample cooling. The peak X-ray power density of 0.5 W/cm^2, indicated by the blue star, is below the thermal damage threshold, which excludes sample heating as an X-ray damage mechanism. For the higher X-ray fluences encountered at free-electron lasers (FEL) or when using pink beam mode at synchrotrons [36], sample damage due to sample heating by X-rays will occur and the gas cell will help to mitigate this radiation damage.

For the static thermal signal as a function of cell parameter at 10.4 kHz, additional data from an earlier ZnO experiment at the same beamline and laser system on 50 nm SiN_x are shown in black in Fig. 6(c). This data includes two measurements: one with an evacuated cell and one with 2 mbar of helium but no flow. The reduction of the thermal signal without helium compared

Optics EXPRESS

to a static helium pressure of 2 mbar amounts to a factor of 4. At 30 ml/min, the thermal signal decreases by a factor of 22, with diminishing returns at higher flow rates.

3.5. Analytical model for the integrated heating measurement

To obtain the relationship between the observed absorption change ΔA in the integrated heating measurements and the temperature increase T(t) in XTA experiments, the results are modeled using Newton's Law of Cooling. We derive the following expressions for ΔA in the integrated heating measurements and the time-dependent temperature T(t) in XTA measurements:

$$\Delta A = \frac{aF\Delta TR}{C\tau} \qquad T(t) = \frac{F\Delta T \exp\left(\tau C\left(\frac{1}{R}-t\right)\right)}{\exp\left(\frac{C\tau}{R}\right)-1} \quad t \in \left[0, \frac{1}{R}\right) \tag{1}$$

Here, t = 0 is the time of the laser interaction with the sample and t = 1/R is the time right before the next laser pulse, R being the laser repetition rate. τ is the coefficient of heat transfer, C is the cell parameter for scaling the coefficient of heat transfer to account for improved cooling by the gas cell, F is the laser fluence, ΔT is the temperature increase per peak fluence and *a* is a scaling factor that connects the temperature increase to the absorption change of the sample ΔA. The derivation is provided in the SI. Compared to the more rigorous method of solving the three-dimensional heat equation, including convection and radiant heat transfer, this simple analytical expression is an approximation. But it is easy to use and can provide estimates of the laser-heating effect across a wide range of laser repetition rates and fluences in thin film XTA experiments.

Applying Eq. (1) to the results in Fig. 6(c), the reduction of the thermal signal by a factor of 22 from no helium to a helium flow of 30 ml/min corresponds to an increase of C by the same factor. By definition, the scaling factor C is equal to one (C = 1) when there is no helium inside the cell. This results in C = 5 at 7 mbar and C = 17 at 101 mbar, which will be used in the subsequent analysis. In the case of gas inside the cell, convection improves the heat dissipation and the data is reproduced by an almost inverse square root scaling of C with the cell pressure P (bP^n, n = -0.46, b = 0.04). Without gas in the cell, no convection is possible and the thermal signal increases sharply.

The static heating as a function of peak power density, Fig. 6(d), is modeled by a global fit with shared a and the values obtained for C, resulting in $\tau = 2042\ s^{-1}$ and $a = 4\ x10^{-4}$ ΔA/K, Fig. 6(d). Since τ and *a* are not independent, the values have a large uncertainty, but we can define a lower limit for τ based on the thermal evaporation of ZnO, which becomes significant around 600 - 670 °C [37,38]. This yields $\tau \geq 2000\ s^{-1,}$ which fits well with the estimated τ. Additionally, the scaling factor *a* has the same order of magnitude as derived from measurements of ZnO at the Zn K-edge [35].

The reduction of static heating for a higher C parameter remains constant across different peak power densities and depends only slightly on the repetition rate, being more effective at 10.4 kHz (factor 1.5). This difference is likely due to the temperature dependence of τ [39,40]. As a result, the magnitude of sample heating in the integrated heating measurements is primarily determined by the peak power density.

4. Discussion of sample heating in XTA experiments

Sample heating in XTA experiments for a wide range of laser repetition rates, fluences and cell parameters can be estimated using the analytical expression from Eq. (1) with the parameters obtained from the integrated temperature measurements of ZnO. As both the magnitude and the temperature dependence of the scaling factor *a* are sample-dependent and different sample preparation methods also affect the scaling factor *a* and the coefficient of heat transfer τ, the following results are strictly speaking only valid for this specific ZnO sample. However, we expect the effectiveness of the cell to be similar for most thin-film samples, as the increased heat

Optics EXPRESS

dissipation is due to improved convection over the entire sample surface, which dominates in comparison to the thermal conductivity through the small sample cross-section Therefore, if the scaling factor a and the coefficient of heat transfer τ can be estimated for the sample of interest, Eq. (1) can be used to decide if heat effects will become critical. The parameters obtained from the ZnO sample are therefore used as a representative example to demonstrate the effect of the gas cell on sample heating in thin-film XTA measurements.

The isolated temperature increase by static heating (t = 1/R) as a function of repetition rate for different fluences is shown in the left of Fig. 7. Although there is no threshold value for static heating, for the following discussion, we define a sample temperature increase of 1 K as the transition point from dynamic to static heating (indicated by the dashed line), which corresponds to an absorption change of 4×10^{-4} A for the ZnO sample. For 10 mJ/cm^2 and C = 1 the transition occurs around 0.45 kHz, for 1 mJ/cm^2 the transition from dynamic to static heating is around 0.9 kHz and for 0.1 mJ/cm^2 around 3.2 kHz. For C > 1, the maximum repetition rate without static heating occurs at C times higher repetition rates for all fluences, e.g., around 20 kHz for 1 mJ/cm^2 and C = 22, which is the maximum achievable value with the current gas cell. Higher repetition rates should be avoided because, even with the cell, the sample would accumulate significant static heating.

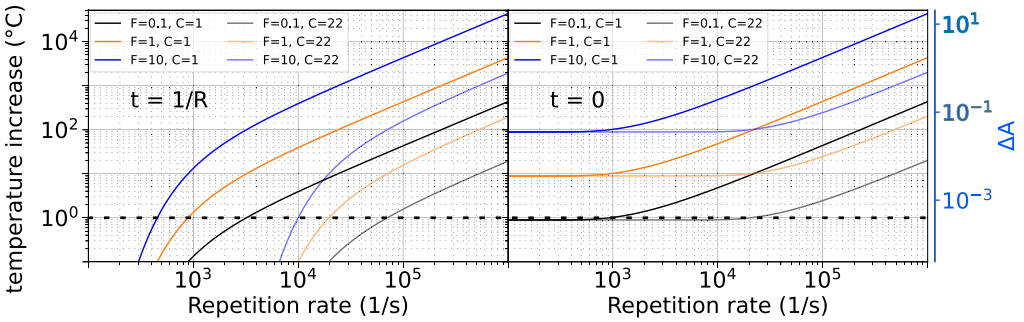

Fig. 7. Simulated ZnO temperature increase as a function of repetition rate for isolated static heating t = 1/R (left) and including dynmic heating t = 0 (right), for three fluences of F = 0.1, 1 and 10 mJ/cm^2 and cell parameters C = 1 (no gas cooling) and C = 22 (best gas cooling achieved with the gas cell). The right y-axis shows the corresponding temperature-induced absorption change.

For t = 0, the time range where XTA experiments are performed, the sample temperature is a combination of static and dynamic heating, right side of Fig. 7. Because the cell only reduces static heating, the absolute temperature improvements by the cell are reduced and significant sample heating is already present at 1 mJ/cm^2 for all repetition rates due to dynamic heating.

When an XTA measurement with a high C-value and a repetition rate slightly below the transition point is subtracted from an identical measurement with a low C-value, all spectral differences are caused solely by static heating and the spectral shape of the thermal signal is obtained. Compared to static temperature measurements with the heating cell, the thermal signal is obtained at the same sample position and under identical experimental conditions, with the disadvantage that the exact sample temperature is unknown. For both methods, the magnitude of the thermal signal must still be matched to the XTA data to correctly remove the thermal contribution.

The analysis shows that the reduction of static heating in the integrated static heating measurements directly translates to improvements in XTA experiments. Compared to a sample in vacuum, measurements with the gas cell allow for up to a factor of 22 times higher repetition rates without static heating in XTA experiments. The optimal ratio of thermal to non-thermal

Optics EXPRESS

signals in XTA experiments is achieved at repetition rates near the transition between dynamic and static heating. This optimal repetition rate can be identified through integrated heating measurements in combination with the presented model. Additionally, X-ray and laser-induced sample damage in XTA experiments can be quantified within a few minutes for a single set of laser and cell parameters. These measurements are therefore ideally suited to become a routine procedure in XTA experiments.

The analysis also showed that static heating of the sample can be reduced to negligible values, especially with the gas cell, but sample heating due to dynamic heating is unavoidable. Therefore, as long as the sample has a temperature-dependent absorption, all XTA results contain thermal artifacts. These must be removed during data evaluation, for example, with static temperature measurements using the presented heating cell or measurements with different gas cell parameters.

5. Conclusions and outlook

The two presented in-vacuum sample cells allow temperature control in XAS and XTA experiments. The heating cell, based on radiative heat exchange, enables homogeneous sample heating for temperature-dependent XAS investigations. These are required to disentangle the thermal signal in XTA experiments. With the heating cell, such measurements also become feasible with laboratory setups – effectively paving the way to perform temperature studies as a standard pre-characterization before or during beamtime at synchrotron radiation or FEL facilities.

The presented gas cell uses continuous gas flow for convective heat dissipation. Measurements of a 290 nm ZnO film show a 22-fold reduction in static heating compared to a ZnO film in vacuum. This allows for a correspondingly higher laser repetition rate, which directly translates into a higher SNR in XTA experiments. Additionally, both X-ray- and laser-induced sample damage of the ZnO film is reduced by factors of 4 and 2, respectively. Due to their small size and high vacuum compatibility, both cells can be integrated into most existing setups without further modifications.

The presented model for interpreting the integrated heating measurements enables a fast and direct estimation of the magnitude of static heating in the XTA experiment, allowing the optimization of laser and cell parameters. Additionally, with the integrated measurement laser- and X-ray-induced sample damage can be characterized.

The combination of heat mitigation with the gas cell and static temperature studies with the heating cell will minimize sample heating and enable the removal of the remaining thermal signal in XTA experiments. We suggest that the presented cells and characterization measurements become a standard part of XTA measurements, which will have a significant impact on future developments of XTA experiments at synchrotron and FEL beamlines, as well as high-repetition rate laboratory setups.

Besides the applications in XTA experiments, both cells can also be used for independent temperature-dependent measurements, such as studying phase transitions or thermal degradation. Here, the temperature range of the heating cell could be extended above 500 °C by using a steel body. Sample cooling to -50°C can be achieved using Peltier coolers.

With the gas cell, temperature-dependent measurements can be combined with experiments at ambient pressure or above ambient pressure and electronic contacts would enable electrocatalysis experiments. This will transform the cells into versatile, easy-to-implement operando sample environments for soft and hard X-ray experiments.

Funding. Open Access Publication Fund of Technische Universität Berlin.

Acknowledgment. We acknowledge support by the Open Access Publication Fund of TU Berlin. We thank Rolf Mitzner and Christian Weniger (Helmholtz Zentrum Berlin, HZB) for the support during the preliminary laser heating investigation. We thank Denny Sommer (Max-Born-Institut für Nichtlineare Optik und Kurzzeitspektroskopie, MBI) for the preparation of the Al thin films. We thank the company NTT-AT for providing the SiC membranes. Measurements were carried out at the UE52-SGM beamline at the BESSY II electron storage ring operated by the Helmholtz Zentrum

Optics EXPRESS

Berlin für Materialien und Energie. We thank Josh Vura-Weis for initial discussions on sample heating and gas cell design.

Disclosures. The authors declare no conflicts of interest.

Data availability. Data underlying the results presented in this paper are not publicly available at this time but may be obtained from the authors upon reasonable request.

Supplemental document. See Supplement 1 for supporting content.

References

1. L. X. Chen and J. Yano, "Deciphering Photoinduced Catalytic Reaction Mechanisms in Natural and Artificial Photosynthetic Systems on Multiple Temporal and Spatial Scales Using X-ray Probes," Chem. Rev **124**(9), 5421–5469 (2024).
2. A. Nilsson, "Time-resolved x-ray absorption spectroscopy probe in ultrafast surface chemistry," Struct. Dyn **12**(1), 011301 (2025).
3. D. Garratt, L. Misiekis, D. Wood, *et al.*, "Direct observation of ultrafast exciton localization in an organic semiconductor with soft X-ray transient absorption spectroscopy," Nat Commun **13**(1), 3414 (2022).
4. H. Stiel, J. Braenzel, A. Jonas, *et al.*, "Towards Understanding Excited-State Properties of Organic Molecules Using Time-Resolved Soft X-ray Absorption Spectroscopy," Int. J. Mol. Sci. **22**(24), 13463 (2021).
5. C. P. Schwartz, F. Ponce, S. Friedrich, *et al.*, "Temperature and radiation effects at the fluorine K-edge in LiF," J. Electron Spectrosc. Relat. Phenom. **218**, 30–34 (2017).
6. U. Ritzmann, P. M. Oppeneer, and P. Maldonado, "Theory of out-of-equilibrium electron and phonon dynamics in metals after femtosecond laser excitation," Phys. Rev. B **102**(21), 214305 (2020).
7. M. Zürch, H.-T. Chang, L. J. Borja, *et al.*, "Direct and simultaneous observation of ultrafast electron and hole dynamics in germanium," Nat Commun **8**(1), 15734 (2017).
8. A. Atkinson, "Transport processes during the growth of oxide films at elevated temperature," Rev. Mod. Phys **57**(2), 437–470 (1985).
9. K. Diller, F. Klappenberger, F. Allegretti, *et al.*, "Investigating the molecule-substrate interaction of prototypic tetrapyrrole compounds: Adsorption and self-metalation of porphine on Cu(111)," The Journal of Chemical Physics **138**(15), 154710 (2013).
10. M. F. Jager, C. Ott, C. J. Kaplan, *et al.*, "Attosecond transient absorption instrumentation for thin film materials: Phase transitions, heat dissipation, signal stabilization, timing correction, and rapid sample rotation," Rev. Sci. Instrum **89**(1), 013109 (2018).
11. D. Garratt, M. Matthews, and J. Marangos, "Toward ultrafast soft x-ray spectroscopy of organic photovoltaic devices," Struct. Dyn **11**(1), 010901 (2024).
12. L. Le Guyader, A. Eschenlohr, M. Beye, *et al.*, "Photon-shot-noise-limited transient absorption soft X-ray spectroscopy at the European XFEL," J Synchrotron Rad **30**(2), 284–300 (2023).
13. D. Filippetto, P. Musumeci, R. K. Li, *et al.*, "Ultrafast electron diffraction: Visualizing dynamic states of matter," Rev. Mod. Phys **94**(4), 045004 (2022).
14. F.-C. Kühl, M. Müller, M. Schellhorn, *et al.*, "Near-edge x-ray absorption fine structure spectroscopy at atmospheric pressure with a table-top laser-induced soft x-ray source," Journal of Vacuum Science & Technology A **34**(4), 041302 (2016).
15. M.-F. Lin, M. A. Verkamp, J. Leveillee, *et al.*, "Carrier-Specific Femtosecond XUV Transient Absorption of PbI2 Reveals Ultrafast Nonradiative Recombination," J. Phys. Chem. C **121**(50), 27886–27893 (2017).
16. R. Ash, Z. Abhari, R. Candela, *et al.*, "X-FAST: A versatile, high-throughput, and user-friendly XUV femtosecond absorption spectroscopy tabletop instrument," Rev. Sci. Instrum **94**(7), 073004 (2023).
17. H. Ftouni, C. Blanc, A. Sikora, *et al.*, "Thermal conductivity measurement of suspended Si-N membranes from 10 K to 275 K using the 3ω-Völklein method," J. Phys.: Conf. Ser **395**(1), 012109 (2012).
18. N. Stojanovic, J. Yun, E. B. K. Washington, *et al.*, "Thin-Film Thermal Conductivity Measurement Using Microelectrothermal Test Structures and Finite-Element-Model-Based Data Analysis," J. Microelectromech. Syst. **16**(5), 1269–1275 (2007).
19. A. Jain and K. E. Goodson, "Measurement of the Thermal Conductivity and Heat Capacity of Freestanding Shape Memory Thin Films Using the 3ω Method," J. Heat Transfer **130**(10), 102402 (2008).
20. W. Xu, X. Wang, X. Zhao, *et al.*, "Determination of Thermal Conductivities for Thin-Film Materials in CMOS MEMS Process," IEEE Trans. Instrum. Meas. **70**, 1–9 (2021).
21. S. R. Choi, D. Kim, S.-H. Choa, *et al.*, "Thermal Conductivity of AlN and SiC Thin Films," Int J Thermophys **27**(3), 896–905 (2006).
22. T. Jeong, J.-G. Zhu, S. Mao, *et al.*, "Thermal Characterization of SiC Amorphous Thin Films," Int. J. Thermophys. **33**, 1000–1012 (2012).
23. Z. Cheng, J. Liang, K. Kawamura, *et al.*, "High thermal conductivity in wafer-scale cubic silicon carbide crystals," Nat Commun **13**(1), 7201 (2022).
24. A. Jonas, K. Dammer, H. Stiel, *et al.*, "Transient Sub-nanosecond Soft X-ray NEXAFS Spectroscopy on Organic Thin Films," Anal. Chem **92**(23), 15611–15615 (2020).

Optics EXPRESS

25. D. Walke, A. Koç, F. Gores, *et al.*, "High-average-power, few-cycle, 2.1 µm OPCPA laser driver for soft-X-ray high-harmonic generation," Opt. Express, OE **33**(5), 10006–10019 (2025).
26. M. Seidel, F. Pressacco, O. Akcaalan, *et al.*, "Ultrafast MHz-Rate Burst-Mode Pump–Probe Laser for the FLASH FEL Facility Based on Nonlinear Compression of ps-Level Pulses from an Yb-Amplifier Chain," Laser Photonics Rev. **16**(3), 2100268 (2022).
27. D. Grötzsch, C. Streeck, C. Nietzold, *et al.*, "A sealable ultrathin window sample cell for the study of liquids by means of soft X-ray spectroscopy," Rev. Sci. Instrum. **88**(12), 123112 (2017).
28. C. Streeck, D. Grötzsch, J. Weser, *et al.*, "In situ gas cell for the analysis of adsorption behaviour on surfaces using X-ray spectroscopy," Appl. Surf. Sci. **609**, 155179 (2023).
29. S. Praetz, D. Grötzsch, C. Schlesiger, *et al.*, "In situ heating cell for temperature dependent transmission x-ray absorption spectroscopy (XAS) measurement with a laboratory based spectrometer," Rev. Sci. Instrum. **96**(3), 035120 (2025).
30. A. Jonas, H. Stiel, L. Glöggler, *et al.*, "Towards Poisson noise limited optical pump soft X-ray probe NEXAFS spectroscopy using a laser-produced plasma source," Opt. Express, OE **27**(25), 36524–36537 (2019).
31. R. Gnewkow, H. Stiel, A. Jonas, *et al.*, "Laboratory soft X-ray setup for transient absorption experiments in the liquid phase using a laser-produced plasma source," Optica, OPTICA **11**(6), 744–752 (2024).
32. M. Nagasaka, T. Hatsui, T. Horigome, *et al.*, "Development of a liquid flow cell to measure soft X-ray absorption in transmission mode: A test for liquid water," J. Electron Spectrosc. Relat. Phenom. **177**(2-3), 130–134 (2010).
33. P. S. Miedema, W. Quevedo, and M. Fondell, "The variable polarization undulator beamline UE52 SGM at BESSY II," Journal of large-scale research facilities JLSRF **2**, A70 (2016).
34. M. Fondell, S. Eckert, R. M. Jay, *et al.*, "Time-resolved soft X-ray absorption spectroscopy in transmission mode on liquids at MHz repetition rates," Struct. Dyn. **4**(5), 054902 (2017).
35. T. C. Rossi, L. Qiao, C. P. Dykstra, *et al.*, "Dynamic control of X-ray core-exciton resonances by Coulomb screening in photoexcited semiconductors," Commun Mater **6**(1), 191 (2025).
36. S. Peredkov, N. Pereira, D. Grötzsch, *et al.*, "PINK: a tender X-ray beamline for X-ray emission spectroscopy," J Synchrotron Rad **31**(3), 622–634 (2024).
37. Z. Wang, J. Byun, S. Lee, *et al.*, "Vacancy driven surface disorder catalyzes anisotropic evaporation of ZnO (0001) polar surface," Nat Commun **13**(1), 5616 (2022).
38. D. Kohl, M. Henzler, and G. Heiland, "Low temperature sublimation processes from clean cleaved polar surfaces of zinc oxide crystals during first heating," Surf. Sci. **41**(2), 403–411 (1974).
39. X. Wu, J. Lee, V. Varshney, *et al.*, "Thermal Conductivity of Wurtzite Zinc-Oxide from First-Principles Lattice Dynamics – a Comparative Study with Gallium Nitride," Sci Rep **6**(1), 22504 (2016).
40. J. Alvarez-Quintana, E. Martínez, E. Pérez-Tijerina, *et al.*, "Temperature dependent thermal conductivity of polycrystalline ZnO films," J. Appl. Phys **107**(6), 063713 (2010).